Biochemical Pharmacology 82 (2011) 1910–1918

Contents lists available at SciVerse ScienceDirect

Biochemical Pharmacology

journal homepage: www.elsevier.com/locate/biochempharm

Influence of the N-terminus and the E2-loop onto the binding kinetics of the antagonist mepyramine and the partial agonist phenoprodifen to H_1R

Hans-Joachim Wittmann [a], Roland Seifert [b], Andrea Strasser [c,*]

[a] Faculty of Chemistry and Pharmacy, University of Regensburg, D-93040 Regensburg, Germany
[b] Institute of Pharmacology, Medical School of Hannover, D-30625 Hannover, Germany
[c] Department of Pharmaceutical and Medicinal Chemistry II, School of Pharmacy, University of Regensburg, D-93040 Regensburg, Germany

ARTICLE INFO

Article history:
Received 8 August 2011
Accepted 7 September 2011
Available online 16 September 2011

Keywords:
Histamine H_1 receptor
Binding kinetics
Gibbs energy
Extracellular surface
Molecular modelling
Molecular dynamics

ABSTRACT

Numerous competitive radioligand binding studies revealed significant differences between human and guinea pig histamine H_1-receptors (hH_1R and gpH_1R), e.g. for the partial H_1R agonist phenoprodifen. But until now, there are only few studies with regard to binding kinetics at H_1R. Previous studies from our group revealed an influence of the exchange of N-terminus and E2-loop between hH_1R and gpH_1R onto affinity of phenoprodifen to H_1R (Strasser A, Wittmann HJ, Seifert R, J Pharmacol Exp Ther 326:783–791, 2008). The aim of this study was, therefore, to examine the impact of the N-terminus and the E2-loop on binding kinetics of the H_1R. The wild type hH_1R and gpH_1R and the chimeric $h_{gpE2}H_1R$ (E2-loogp from guinea pig) and $h_{gpNgpE2}H_1R$ (N-terminus and E2-loop from guinea pig) were co-expressed with regulator of G-protein signaling protein RGS4 in Sf9 insect cells and kinetic binding studies were performed using the antagonist [^{3}H]mepyramine as radioligand. The rate constants for association and dissociation were, in dependence of the ligand, different between hH_1R and gpH_1R. Furthermore, the rate constants for association at $h_{gpNgpE2}H_1R$ were significantly different compared to hH_1R and gpH_1R. Molecular dynamic simulation studies detected different interactions of amino acid side chains on the extracellular surface of the receptor. Based on these findings, the influence of extracellular surface onto binding kinetics and binding affinity can be explained. Thus, the extracellular surface of G protein-coupled receptors for biogenic amines, exhibits influence onto kinetics of ligand binding, onto ligand recognition and ligand guiding into the binding pocket.

1. Introduction

The histamine H_1-receptor (H_1R) [1] is a biogenic amine receptor and belongs to the G protein-coupled receptors (GPCRs) [2,3]. H_1R antagonists have clinical relevance in treatment of allergic diseases, whereas H_1R agonists are important tools to obtain a more detailed insight with regard to ligand–receptor-interaction. Many studies were performed in order to determine affinities, potencies and efficacies of several compounds at different H_1R species orthologs under steady-state conditions [4–8]. Histaprodifens were originally identified as potent H_1R agonists at guinea-pig ileum [9,10]. For some histaprodifens, like suprahistaprodifen, phenoprodifen and dimeric histaprodifen, large species-differences were found between hH_1R and gpH_1R [4,6]. Extensive site-directed mutagenesis and molecular modelling studies were performed in order to obtain more detailed insights into ligand–receptor interaction on molecular level [5–8,11–13]. Recently, the crystal structure of the human H_1R in complex with the antagonist doxepin has been resolved [14].

While currently, there is a strong focus on structural aspects in GPCR research, relatively little work is being conducted on thermodynamics although analysis of these parameters provides important insights into mechanisms of ligand/receptor interaction, specifically when thermodynamics calculations are combined with radioligand binding studies, site-directed mutagenesis and molecular modelling based on the numerous new active- and inactive state GPCR crystal structures [15,16].

We have recently characterized H_1R thermodynamically with regard to enthalpy and entropy of binding of antagonists as well as of agonists [17]. No differences in binding enthalpy, or binding entropy, respectively, were found for mepyramine between hH_1R and gpH_1R. In contrast, significant differences in binding enthalpy or entropy between hH_1R and gpH_1R were observed for

Abbreviations: E2 loop, second extracellular loop; gp, guinea-pig; GPCR, G protein-coupled receptor; h, human; $h_{gpE2}H_1R$, human histamine H_1R with gp E2-loop; $h_{gpNgpE2}H_1R$, human histamine H_1R with gp N-terminus and gp E2-loop; H_1R, histamine H_1 receptor; MEP, mepyramine.

* Corresponding author at: Department of Pharmaceutical and Medicinal Chemistry II, University of Regensburg, Universitätsstrasse 31, D-93053 Regensburg, Germany. Tel.: +49 941 943 4821; fax: +49 941 943 4820.
E-mail address: andrea.strasser@chemie.uni-regensburg.de (A. Strasser).

0006-2952/$ – see front matter © 2011 Elsevier Inc. All rights reserved.
doi:10.1016/j.bcp.2011.09.005

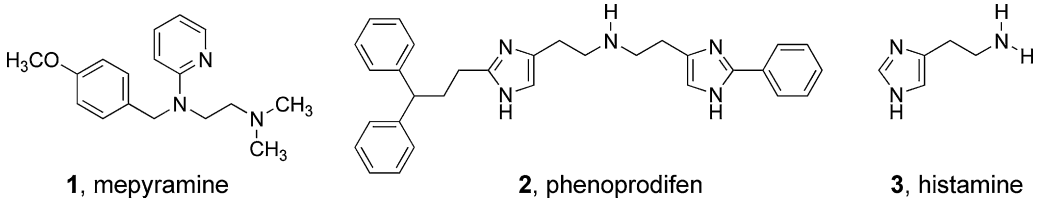

Fig. 1. Structures of mepyramine and phenoprodifen. Mepyramine **1**, phenoprodifen **2**, histamine **3**.

phenoprodifen [17]. Only few studies analyzed the binding kinetics of H_1R antagonists [18–23].

The first aim of this study was to analyze the binding kinetics of mepyramine **1** and phenoprodifen **2** (Fig. 1) at hH_1R and gpH_1R with regard to species-differences in rate constants of association or dissociation. Previous studies revealed a decrease in affinity of phenoprodifen to a chimeric hH_1R with the gpH_1R-N-terminus and gpH_1R-E2-loop [7]. Moreover, we obtained evidence for a modulatory role of extracellular domains of the H_4R on ligand binding [24]. Furthermore, nuclear magnetic resonance studies with the purified β_2-adrenergic receptor showed an impact of extracellular domains on ligand binding [25]. Thus, the second aim was to study the influence of N-terminus and E2-loop onto binding kinetics of mepyramine and phenoprodifen (Fig. 2).

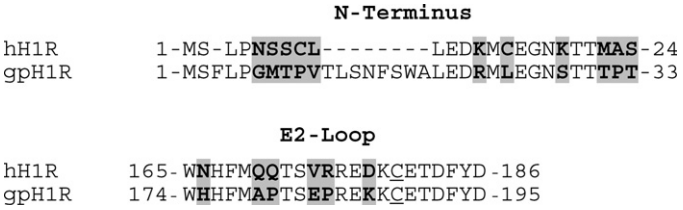

Fig. 2. Amino acid sequence of N-Terminus and E2-Loop of hH_1R and gpH_1R. Bold and grey boxed amino acids indicate different amino acids between hH_1R and gpH_1R in N-Terminus and E2-loop.

2. Materials and methods

2.1. Materials

[^{3}H]mepyramine (30.0 Ci/mmol) was from PerkinElmer Life Sciences (Boston, MA). Rotiszint ecoplus from Roth (Karlsruhe, Germany) was used as liquid scintillation cocktail. Mepyramine and histamine were from Sigma–Aldrich (St. Louis, MO). Phenoprodifen was kindly provided by Dr. Sigurd Elz (Department of Medicinal Chemistry I, University of Regensburg, Germany).

2.2. Preparation of compound stock solutions

Chemical structures of the analyzed compounds are given in Fig. 1. Mepyramine **1** and histamine **3** was dissolved in double-distilled water, resulting in 10 mM stock solutions. Phenoprodifen **2** was dissolved in a solvent mixture containing 30% (v/v) DMSO, 30% (v/v) Tris/HCl pH 7.4 (10 mM) and 40% (v/v) double-distilled water, resulting in a 5 mM stock solution. All dilution series were obtained by dilution with the corresponding solvent: double-distilled water in case of mepyramine and a mixture of 30% (v/v) DMSO, 30% (v/v) Tris/HCl pH 7.4 (10 mM) and 40% (v/v) double-distilled water in case of phenoprodifen.

2.3. Binding assays

For all binding assays, Sf9 cell membranes, expressing the corresponding H_1R and RGS4 were used. The coexpression with RGS4 is necessary to obtain well signals in the steady-state GTPase assay [26]. In order to be able to compare GTPase data with binding data, we use membranes, coexpressing RGS4 also in the binding assay. The RGS4 has no influence onto ligand affinity. All binding assays were performed, as described previously [6]. Shortly, the membranes were thawed, suspended in binding buffer (12.5 mM $MgCl_2$, 1 mM EDTA, 75 mM Tris–HCl, pH 7.4) and sedimented by centrifugation for 10 min at 4 °C and 13,000 × g. Afterwards, the membrane pellets were resuspended in binding buffer. Each reaction mixture contained about 50–75 μg of membrane protein. The final pH in each reaction mixture, containing membrane, [^{3}H]mepyramine and ligand is about 7.4. After performing the kinetic binding assay at a temperature of 20 °C, as described below in more detail, the bound [^{3}H]mepyramine was separated from free [^{3}H]mepyramine by filtration through GF/C (Whatman, Maidstone, UK). Subsequently, three washing steps with 2 ml binding buffer (4 °C) were performed. Liquid scintillation counting was used to determine the radioactivity, remaining on the filters.

2.4. Measurement of association and dissociation binding kinetics

The association binding kinetics of [^{3}H]mepyramine were performed with final [^{3}H]mepyramine concentrations of 3 nM, 5 nM, 7.5 nM and 10 nM. All assays were carried out three times with Sf9 cell membranes expressing the corresponding H_1R ortholog and RGS4. Membranes were used from three different independent membrane preparations. The association kinetics were observed within 15 min. Within the first 3.5 min, time steps between 5 and 10 s were recorded. Within 3.5 to 5.0 min, every 30 s a measurement was performed. From 5 min up to 15 min, the measurement was performed every minute.

The dissociation kinetics of [^{3}H]mepyramine were performed with a final [^{3}H]mepyramine concentration of 5 nM in presence of 1 μM mepyramine. All assays were carried out three times with Sf9 cell membranes expressing the corresponding H_1R and RGS4. Membranes were used from three independent membrane preparations. The dissociation kinetics was observed within 30 min at distinct times.

The competitive association binding kinetics were performed with a final [^{3}H]mepyramine concentration of 5 nM. The competitive association kinetics were observed within 30 min at the following times: 0.5, 1, 2, 4, 6, 8, 10, 15, 20, 25 and 30 min. Within each assay we analyzed four different concentrations of the unlabelled ligand. The following final concentrations of unlabelled ligand were used at hH_1R and $h_{gpNgpE2}H_1R$. Phenoprodifen **2** was analyzed at 100 nM, 1 μM, 3.16 μM and 10 μM. The following final concentrations of unlabelled ligand were used at gpH_1R. Phenoprodifen **2** was analyzed at 31.6 nM, 100 nM, 316 nM and 500 nM. Histamine **3** was analyzed at 316 nM, 1 μM, 3.16 μM and 10 μM at hH_1R and gpH_1R. All assays were performed three times with Sf9 cell membranes expressing the corresponding H_1R and RGS4. Membranes were used from three independent membrane preparations.

2.5. Calculation of rate constants for binding of [^{3}H]mepyramine

For the binding kinetics of the radioligand [^{3}H]mepyramine the equilibrium

$$A + R \rightleftharpoons AR \quad (1)$$

is formulated. Therein, A represents the radioligand, whereas R defines the receptor, AR is the radioligand–receptor complex. The differential equation for formation of AR is given by

$$\frac{\partial AR(t)}{\partial t} = k_1(A_0 - AR(t))(R_0 - AR(t)) - k_2 AR(t) \quad (2)$$

Therein, k_1 is the rate constant for association and k_2 the rate constant for dissociation. A_0 and R_0 are the initial concentrations of A and R. Rate constants were determined according to Motulsky and Mahan [27].

2.6. Calculation of rate constants for binding of non-labelled ligands in presence of a radioligand

For the competition binding kinetics of a radioligand and a non-labelled ligand L, the following equations was formulated:

$$A + R \rightleftharpoons AR \quad (3)$$

$$L + R \rightleftharpoons LR \quad (4)$$

The corresponding differential equations are given by:

$$\frac{\partial AR(t)}{\partial t} = k_1(A_0 - AR(t))(R_0 - AR(t) - LR(t)) - k_2 AR(t) \quad (5)$$

$$\frac{\partial LR(t)}{\partial t} = k_3(L_0 - LR(t))(R_0 - AR(t) - LR(t)) - k_4 LR(t) \quad (6)$$

Therein, k_3 is the rate constant of association and k_4 the rate constant of dissociation for the formation of LR. L_0 is the initial concentration of the unlabelled ligand. Rate constants were determined according to Motulsky and Mahan [27].

2.7. Kinetics of non-specific binding of [^{3}H]mepyramine

Kinetics of non-specific binding of [^{3}H]mepyramine were determined in presence of 1 μM unlabelled mepyramine. Within the first 3 min, the time steps were ~10 s, from 3 min up to ~15 min, the time steps were ~60 s. The non-specific binding reached a plateau already at 10 s. All kinetic data were corrected for non-specific binding by substraction of the corresponding value at 10 s.

2.8. Calculation of Gibbs energy of activation

The Eyring-equation, developed within the concept of transition state theory [28,29] is given by

$$k_1 = \frac{k_B T}{hc^o} \exp\left(-\frac{\Delta G^{\neq}_{ass}}{RT}\right) \quad (7)$$

for the association process of a ligand into the binding pocket of a receptor. Therein, $\Delta G^{\neq}_{ass}$ describes the change in Gibbs energy of activation during the ligand binding and c^o denotes the reference concentration of 1 mol/l. The corresponding dissociation process is described by

$$k_2 = \frac{k_B T}{h} \exp\left(-\frac{\Delta G^{\neq}_{diss}}{RT}\right) \quad (8)$$

Therein, $\Delta G^{\neq}_{diss}$ describes the change in Gibbs energy during dissociation of the ligand–receptor-complex. The change in the Gibbs standard energy, which is related to the equilibrium constant of ligand binding to a receptor is given by

$$\Delta G^{\circ} = -RT \ln(K) = \Delta G^{\neq}_{ass} - \Delta G^{\neq}_{diss} \quad (9)$$

2.9. Molecular modelling

For molecular modelling of the inactive H_1R, the crystal structure of hH_1R was used as template [14] to model inactive hH_1R, $h_{gpNgpE2}H_1R$ and gpH_1R. The active state models of hH_1R, $h_{gpNgpE2}H_1R$ and gpH_1R were generated using opsin, cocrystallized with a part of Gα, as template [30]. Homology modelling was performed, as already described [7,31]. Mepyramine **1**, a H_1R antagonist was docked into the inactive state models, whereas phenoprodifen **2**, a partial agonist at H_1R was docked into the active state models. Afterwards, molecular dynamic simulations of the receptor models, including the natural surrounding were performed, using protocols as already described [6].

2.10. Miscellaneous

Cell culture and membrane preparations were performed as described [6]. The determination of protein concentration was performed as described previously [4,6]. The [^{3}H]mepyramine binding assays were performed as described [6]. All assays were carried out in parallel and under the same experimental conditions and at 20 °C. All kinetic data were analyzed with the software Prism 5.01 (GraphPad Software Inc., San Diego, CA, USA). Statistical analysis was performed with the software Prism 5.01. All data are the means ± S.E.M. of at least three independent experiments. To compare two pairs of data, the significance of the deviation of zero p was calculated using the t test.

3. Results

3.1. Binding kinetics of mepyramine

The rate constants for association and dissociation for mepyramine are given in Table 1. The corresponding values of

Table 1
Rate constants of association and dissociation of mepyramine at hH_1R, $h_{gpE2}H_1R$, $h_{gpNgpE2}H_1R$ and gpH_1R coexpressed with RGS4 in Sf9 cell membranes. [^{3}H]MEP association binding kinetics in Sf9 membranes expressing hH_1R, $h_{gpE2}H_1R$, $h_{gpNgpE2}H_1R$ and gpH_1R in combination with RGS4 was determined in presence of different [^{3}H]MEP concentrations as described under Section 2. Data were analyzed as described under Section 2. The k_1 and k_2 values are the means ± S.E.M. of three experiments with independent membrane preparations.

	k_1 [l min^{-1} mol^{-1}]	k_2 [min^{-1}]
hH_1R	$7.20 \times 10^7 \pm 0.25 \times 10^7$	0.32 ± 0.01
$h_{gpE2}H_1R$	$9.86 \times 10^7 \pm 0.93 \times 10^7$	0.41 ± 0.04
$h_{gpNgpE2}H_1R$	$9.24 \times 10^7 \pm 0.54 \times 10^7$	0.35 ± 0.02
gpH_1R	$5.84 \times 10^7 \pm 0.38 \times 10^7$	0.15 ± 0.01

Table 2
Calculated $\Delta G^{\neq}_{ass}$, $\Delta G^{\neq}_{diss}$ and ΔG° based on the experimental rate constants of association and dissociation for mepyramine **1**. The calculations were performed according to Eqs. (7)–(9) as described under Section 2.

	$\Delta G^{\neq}_{ass}$ [kJ/mol]	$\Delta G^{\neq}_{diss}$ [kJ/mol]	ΔG° [kJ/mol]
hH_1R	37.64 ± 0.08	84.51 ± 0.08	−46.87 ± 0.16
$h_{gpE2}H_1R$	36.87 ± 0.23	83.91 ± 0.24	−47.07 ± 0.47
$h_{gpNgpE2}H_1R$	37.03 ± 0.14	84.30 ± 0.14	−47.27 ± 0.28
gpH_1R	38.15 ± 0.16	86.36 ± 0.16	−48.21 ± 0.32

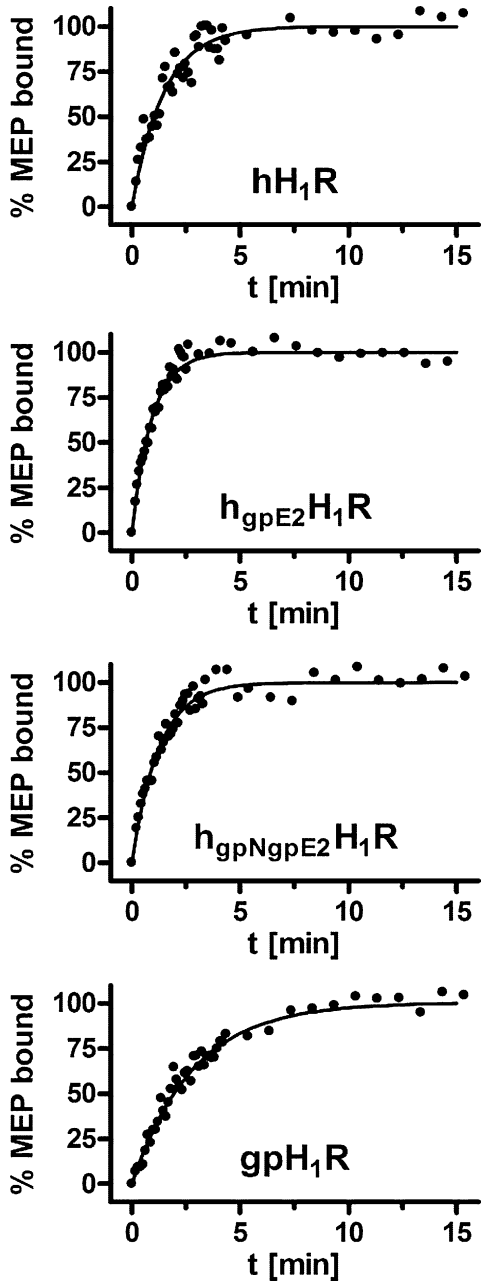

Fig. 3. Association kinetics of [^{3}H]mepyramine at hH_1R, $h_{gpE2}H_1R$ and $h_{gpNgpE2}H_1R$ and gpH_1R. The kinetic binding assays were performed as described under Section 2. The data shown are representative and were performed in presence of 5 nM [^{3}H]mepyramine. The bound [^{3}H]mepyramine is set equal to 100% at equilibrium.

$\Delta G^{\neq}_{ass}$, $\Delta G^{\neq}_{diss}$, and ΔG° are given in Table 2. Representative association kinetics are shown in Fig. 3, and representative dissociation kinetics are shown in Fig. 4. The rate constants for mepyramine are significantly different between hH_1R and gpH_1R (Table 1): At hH_1R, the rate constant for association k_1 is significantly higher ($p = 0.0256$), than at gpH_1R. Also the rate constant for dissociation k_2 is significantly higher ($p = 0.0001$) at hH_1R than at gpH_1R. Additionally, the rate constants at the chimeric $h_{gpE2}H_1R$ and $h_{gNgpE2}H_1R$ are significantly different to the data obtained for hH_1R (Table 1): The rate constants for association of [^{3}H]mepyramine at $h_{gpE2}H_1R$ ($p = 0.0236$) and $h_{gpNgpE2}H_1R$ ($p = 0.0128$) are significantly higher than at hH_1R and not smaller in direction to gpH_1R. The rate constants for dissociation at $h_{gpE2}H_1R$ and $h_{gpNgpE2}H_1R$ are not significantly different. Based on Eq. (7), $\Delta G^{\neq}_{ass}$ was calculated (Table 2). For mepyramine **1**, the values of $\Delta G^{\neq}_{ass}$ are about 37 kJ/mol, whereas values of $\Delta G^{\neq}_{diss}$, determined using Eq. (8), are about 84 kJ/mol at H_1R.

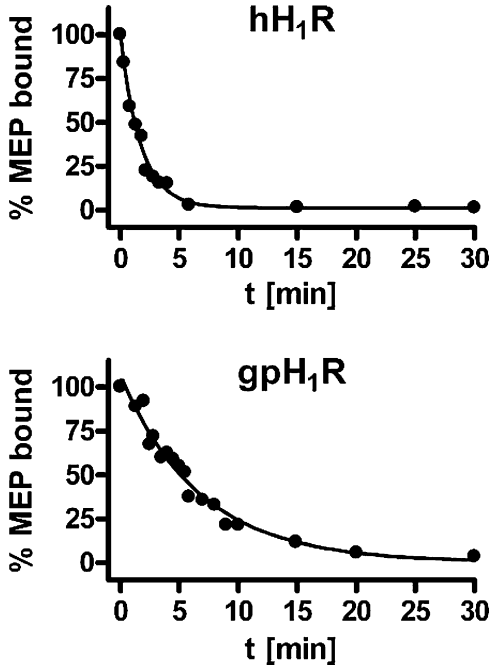

Fig. 4. Dissociation kinetics of [^{3}H]mepyramine at hH_1R and gpH_1R. The kinetic binding assays were performed as described under Section 2. The data shown are representative and were performed in presence of 5 nM [^{3}H]mepyramine and 1 μM mepyramine. The bound [^{3}H]mepyramine is set equal to 100% at $t = 0$.

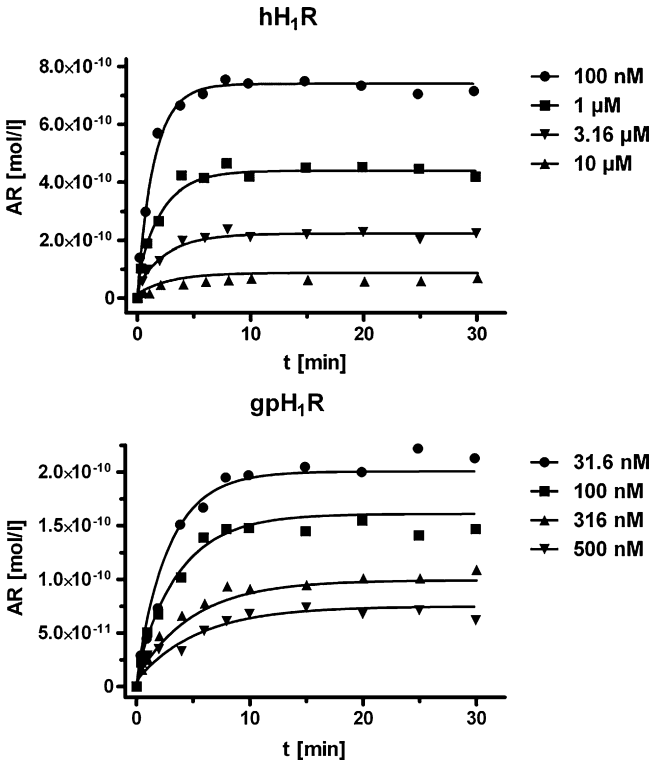

Fig. 5. Association kinetics of [^{3}H]mepyramine to hH_1R and gpH_1R in presence of phenoprodifen **2**. The kinetic binding assays were performed as described under Section 2. The data shown are representative and were performed in presence of 5 nM [^{3}H]mepyramine.

Table 3
Rate constants of association and dissociation of phenoprodifen at hH_1R, $h_{gpNgpE2}H_1R$ and gpH_1R coexpressed with RGS4 in Sf9 cell membranes. [^{3}H]MEP association binding kinetics in Sf9 membranes expressing hH_1R, $h_{gpNgpE2}H_1R$ and gpH_1R in combination with RGS4 was determined in presence of 5 nM [^{3}H]MEP and different concentrations of phenoprodifen as described under Section 2. Data were analyzed as described under Section 2. The k_3 and k_4 values are the means ± S.E.M. of three experiments with independent membrane preparations.

	k_3 [l min^{-1} mol^{-1}]	k_4 [min^{-1}]	pK_i (log(k_3/(k_4 c^o)))	pK_i[a] (comp. bind. ass.)
hH_1R	$3.51 \times 10^6 \pm 0.09 \times 10^6$	2.02 ± 0.07	6.24 ± 0.03	6.60 ± 0.07
$h_{gpNgpE2}H_1R$	$1.80 \times 10^6 \pm 0.50 \times 10^6$	1.97 ± 0.55	5.96 ± 0.24	6.01 ± 0.02
gpH_1R	$2.44 \times 10^7 \pm 0.09 \times 10^7$	2.01 ± 0.13	7.08 ± 0.04	7.33 ± 0.08

[a] Data already published [6,7].

Table 4
Calculated $\Delta G^{\neq}_{ass}$, $\Delta G^{\neq}_{diss}$ and ΔG° based on the experimental rate constants of association and dissociation for phenoprodifen **2**. The calculations were performed according to Eqs. (7)–(9) as described under Section 2.

	$\Delta G^{\neq}_{ass}$ [kJ/mol]	$\Delta G^{\neq}_{diss}$ [kJ/mol]	ΔG° [kJ/mol]
hH_1R	45.00 ± 0.06	80.02 ± 0.08	−35.02 ± 0.14
$h_{gpNgpE2}H_1R$	46.63 ± 0.68	80.08 ± 0.68	−33.45 ± 1.36
gpH_1R	40.28 ± 0.09	80.04 ± 0.16	−39.76 ± 0.25

3.2. Binding kinetics of phenoprodifen

The rate constants for association k_3 and dissociation k_4 of phenoprodifen **2** are given in Table 3. Representative association kinetics are shown in Fig. 5. The corresponding values of $\Delta G^{\neq}_{ass}$, $\Delta G^{\neq}_{diss}$, and ΔG° are given in Table 4. The rate constant of association of phenoprodifen **2** at hH_1R is ~20 smaller than for mepyramine **1**. In contrast, the rate constant of dissociation of phenoprodifen **2** is ~6 higher than of mepyramine **1** at hH_1R. A comparison of the rate constants of association between hH_1R and $h_{gpNgpE2}H_1R$ showed that the rate constant of association is significantly higher at hH_1R than at $h_{gpNgpE2}H_1R$ ($p = 0.0222$). The rate constant of association for phenoprodifen **2** at gpH_1R is ~10-fold higher ($p = 0.0001$) than at hH_1R and $h_{gpNgpE2}H_1R$. Surprisingly, no significant difference between the rate constants for the dissociation of phenoprodifen **2** is found between hH_1R, $h_{gpNgpE2}H_1R$ and gpH_1R. But, compared to mepyramine **1**, the rate constants of dissociation are ~5–15-fold higher. At hH_1R, $\Delta G^{\neq}_{ass}$ has a value of ~45 kJ/mol rising to ~46.6 kJ/mol at $h_{gpNgpE2}H_1R$, whereas, at gpH_1R, $\Delta G^{\neq}_{ass}$ decreased to ~40 kJ/mol. $\Delta G^{\neq}_{ass}$ is ~80 kJ/mol at hH_1R, $h_{gpNgpE2}H_1R$ and gpH_1R.

3.3. Binding kinetics of histamine

The rate constants for association and dissociation and corresponding Gibbs energies of histamine at hH_1R and gpH_1R are given in Table 5. The rate constants for association were not significantly different between hH_1R and gpH_1R and were found in a range of $\sim 1.5 \times 10^6$ to $\sim 2 \times 10^6$ l min^{-1} mol^{-1}. The rate constants for dissociation at hH_1R and gpH_1R were found in a range of ~4–~5 min^{-1} and are not significantly different between hH_1R and gpH_1R. At hH_1R and gpH_1R, $\Delta G^{\neq}_{ass}$ has a value of ~47 kJ/mol, whereas $\Delta G^{\neq}_{diss}$ has a value of ~78 kJ/mol.

4. Discussion

4.1. Binding of [^{3}H]mepyramine to H_1R

The rate constants for association and dissociation of mepyramine, determined within this study at H_1R, are in good accordance to the literature data [19,20,22,23]. Gillard et al. [22,23] analyzed the binding kinetics of several H_1R antagonists at H_1R. They found the rate constants for association in a range from 1.2×10^6 l min^{-1} mol^{-1} up to 5.1×10^8 l min^{-1} mol^{-1}. The rate constants for dissociation are ranged from 0.005 min^{-1} up to 3.3 min^{-1}. Gillard et al. [22,23] determined a rate constant for association of 5.13×10^8 l mol^{-1} min^{-1} and a rate constant for dissociation of 0.86 min^{-1} for meypramine at hH_1R. The slight differences between the literature data and the data of our present study are mainly caused by different assay temperatures. Gillard et al. [22,23] performed the assays at hH_1R at temperatures of 25 °C or 37 °C, whereas the assays within this study are performed at 20 °C. In previous studies, significant differences between the K_D values of [^{3}H]mepyramine between hH_1R and gpH_1R were found [4]. The data obtained within this study indicate that there are also significant differences between hH_1R and gpH_1R in binding kinetics of [^{3}H]mepyramine.

The analysis of the binding kinetics of [^{3}H]mepyramine at the chimeric $h_{gpE2}H_1R$ and $h_{gpNgpE2}H_1R$ shows that the large species-differences in N-terminus and E2-loop between hH_1R and gpH_1R are not responsible for the species-differences between hH_1R and gpH_1R in binding kinetics, because the rate constants for association at $h_{gpE2}H_1R$ and $h_{gpNgpE2}H_1R$ are higher than at hH_1R and gpH_1R. Although the amino acid sequence is increasingly changed into that of gpH_1R in the series $hH_1R \rightarrow h_{gpE2}H_1R \rightarrow h_{gpNgpE2}H_1R \rightarrow gpH_1R$, the rate constants of association do not change in direction to the value at gpH_1R. Based on these data, we suggest that the extracellular part of H_1R, the E2-loop and the N-terminus is not responsible for the significant differences in binding kinetics between hH_1R and gpH_1R. Thus, the differences in amino acid sequence, leading to differences in binding kinetics are presumably located in the transmembrane region.

A comparison of the amino acid sequence of the transmembrane domains exhibits some positions with differences between hH_1R and gpH_1R: $T^{1.41}S$, $I^{1.42}V$, $C^{1.43}S$, $G^{1.48}A$, $N^{2.61}S$, $L^{2.66}H$, $M^{2.67}R$, $F^{4.51}L$, $F^{6.39}C$, $I^{6.53}V$, $H^{7.33}P$, $L^{7.34}V$ and $I^{7.44}L$ (nomenclature according to Ballesteros et al. [32]). Further differences are found

Table 5
Rate constants of association and dissociation and corresponding values of $\Delta G^{\neq}_{ass}$ and $\Delta G^{\neq}_{diss}$ of histamine at hH_1R and gpH_1R coexpressed with RGS4 in Sf9 cell membranes. [^{3}H]MEP association binding kinetics in Sf9 membranes expressing hH_1R or gpH_1R in combination with RGS4 was determined in presence of 5 nM [^{3}H]MEP and different concentrations of histamine as described under Section 2. Data were analyzed as described under Section 2. The k_3 and k_4 values are the means ± S.E.M. of three experiments with independent membrane preparations. $\Delta G^{\neq}_{ass}$ and $\Delta G^{\neq}_{diss}$ were calculated according to Eqs. (7) and (8) as described under Section 2.

	k_3 [l min^{-1} mol^{-1}]	k_4 [min^{-1}]	$\Delta G^{\neq}_{ass}$ [kJ/mol]	$\Delta G^{\neq}_{diss}$ [kJ/mol]
hH_1R	$1.65 \times 10^6 \pm 0.15 \times 10^6$	3.96 ± 0.36	46.84 ± 0.22	78.38 ± 0.22
gpH_1R	$1.79 \times 10^6 \pm 0.24 \times 10^6$	4.91 ± 0.79	46.64 ± 0.33	77.87 ± 0.39

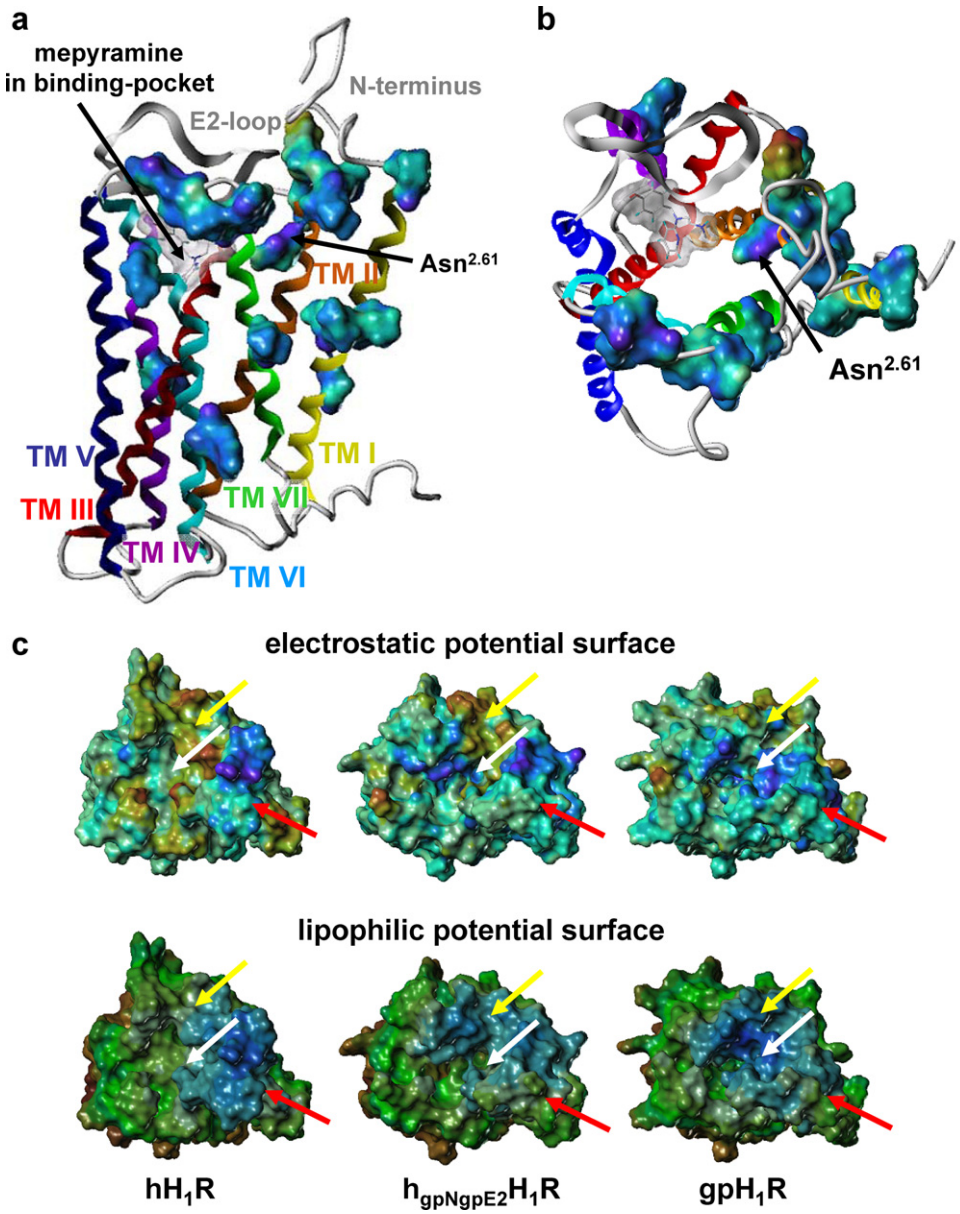

Fig. 6. Differences between hH_1R, $h_{gpNgpE2}H_1R$ and gpH_1R, based on inactive receptor models. (a) Model of inactive hH_1R, with amino acids, different between hH_1R and gpH_1R (side view) indicated by volume surface; differences in N-terminus and E2-loop are not shown; (b) model of inactive hH_1R with amino acids, different between hH_1R and gpH_1R (view from the extracellular part) indicated by volume surface; differences in N-terminus and E2-loop are not shown; c, differences in the electrostatic and lipophilic surface potential between inactive hH_1R, $h_{gpNgpE2}H_1R$ and gpH_1R; yellow arrow: location of E2-loop, red arrow: location of N-terminus, white arrow: entry region into binding pocket; electrostatic potential: blue—negative, red—positive; lipophilic potential: increasing lipophilicity in direction blue → green → brown. (For interpretation of the references to color in this figure legend, the reader is referred to the web version of the article.)

in the extracellular loops E1 and E3. The mentioned differences are shown in Fig. 6a and b. Most of these different amino acids do neither point inward the receptor, nor into the binding pocket, except $Asn^{2.61}$, which is responsible for the species differences in affinity of suprahistaprodifen between hH_1R and gpH_1R [5]. However, the $Asn^{2.61}Ser$ point mutation at hH_1R exhibited no significant change in K_D of mepyramine with regard to wild-type hH_1R [5]. Thus, $Asn^{2.61}Ser$ is not responsible for the species differences in affinity of mepyramine between hH_1R and gpH_1R. Gillard et al. [22] observed at $Lys^{5.39}Ala$ and $Thr^{5.42}Ala$ mutants of hH_1R influence onto rate constants of association and dissociation. A comparison of the rate constants of association or dissociation, respectively, between $h_{gpE2}H_1R$ and $h_{gpNgpE2}H_1R$ reveals no significant differences. Thus, we suggest that the N-terminus has no influence onto binding kinetics of mepyramine at H_1R.

In marked contrast, the E2-loop has a significant influence on mepyramine binding kinetics. In Fig. 6c, the differences in electrostatic and lipophilic surface potential of the extracellular parts between hH_1R, $h_{gpNgpE2}H_1R$ and gpH_1R are shown. As indicated by the arrows (Fig. 6c, white arrows), the differences are located in the region for ligand entry into the binding pocket. Based on these data, the extracellular part may influence ligand recognition and routing the ligand into the binding pocket: At hH_1R, the entry region is more positive compared to gpH_1R. Since the ligand is also positively charged, an interaction of the ligand with the surface of hH_1R cannot be well established, but a faster direction into the negatively charged binding pocket is expected. At gpH_1R, the extracellular surface is more negatively charged. Thus, the ligand can interact well with the extracellular surface. But, due to the negative surface charge the direction of the ligand

into the binding pocket is expected to be slower, than in case of hH_1R. In the chimeric $h_{gpNgpE2}H_1R$, there are positively and negatively charged regions on the extracellular surface. Thus, on the one hand, the ligand can be captured, and on the other hand, the ligand can be directed into the negative charged binding pocket. Thus, the influence of E2-loop onto rate constant of association can be explained. In general, electrostatic and lipophilic surface potential can be used to explain association kinetics.

4.2. Binding of phenoprodifen to H_1R

The rate constant for association and dissociation of the partial agonist phenoprodifen at H_1R are in the same range as already found for antagonists at guinea-pig, rat, rabbit and human H_1R [18–23]. The data revealed a significant difference in association kinetics of **2** between hH_1R and gpH_1R (Table 3). As already observed for mepyramine, the exchange of the N-Terminus and E2-loop had significant influence onto association kinetics, but in the series $hH_1R \rightarrow h_{gpNgpE2}H_1R \rightarrow gpH_1R$, the rate constant of association, does not alter in direction of gpH_1R. Based on this result, we suggest that the extracellular part has an influence onto the association kinetics, but is not responsible for the observed species-differences in association kinetics between hH_1R and gpH_1R. Thus, other amino acid differences between hH_1R and gpH_1R are, as already mentioned above, responsible for the observed species-differences. In contrast to association kinetics, no significant difference in rate constants of dissociation for phenoprodifen **2** at hH_1R, $h_{gpNgpE2}H_1R$ and gpH_1R was observed. Since a similar result was obtained for mepyramine **1**, it can be suggested, that the N-terminus and E2-loop have no influence onto dissociation kinetics.

The different interactions between charged amino acids at the extracellular part of the H_1R–phenoprodifen-complex is illustrated in Fig. 7. An electrostatic interaction between Asp186 and $Lys^{5.39}$, between Asp183 and Lys442 is found at hH_1R. Analogous interactions were observed at $h_{gpNgpE2}H_1R$ and gpH_1R. At gpH_1R, a more negative value of ΔG°, compared to hH_1R and $h_{gpNgpE2}H_1R$ was observed (Table 4). This can be explained by differences in interaction of Glu190 (gpH_1R) (corresponds to Glu181 at hH_1R). At gpH_1R, this glutamate interacts electrostatically with the ligand in the binding pocket, whereas no interaction with the N-terminus could be detected. In contrast, at hH_1R, the glutamate side chain is moved away from the ligand in direction to Lys13 (N-terminus) (corresponds to Arg22 at gpH_1R). Thus, the interaction of Lys13 with the ligand in the binding pocket is reduced, leading to a more positive ΔG° (Table 4). At $h_{gpNgpE2}H_1R$, the distance between glutamate and the ligand is larger, whereas the distance between the glutamate and Arg22 is smaller, than at hH_1R. Thus, there is no interaction between the glutamate and the ligand, resulting in a more positive ΔG°, than at hH_1R (Table 4).

Since phenoprodifen **2** is, like mepyramine **1**, positively charged, the electrostatic potential on the receptor surface should have the same influence onto association of phenoprodifen (Fig. 6c). But, in comparison to mepyramine, phenoprodifen is more lipophilic. Thus, an influence of the lipophilic surface potential (Fig. 6c) cannot be neglected. At hH_1R, the extracellular surface is more lipophilic, than at gpH_1R. Accordingly, the lipophilic parts of phenoprodifen can interact well with the extracellular surface at hH_1R. Due to this well-established interaction, it can be suggested that the direction of the phenoprodifen, due to lipophilicity, is directed slower into the binding pocket, than at gpH_1R. Furthermore, it has to be taken into account, that the differences in extracellular surface may result in

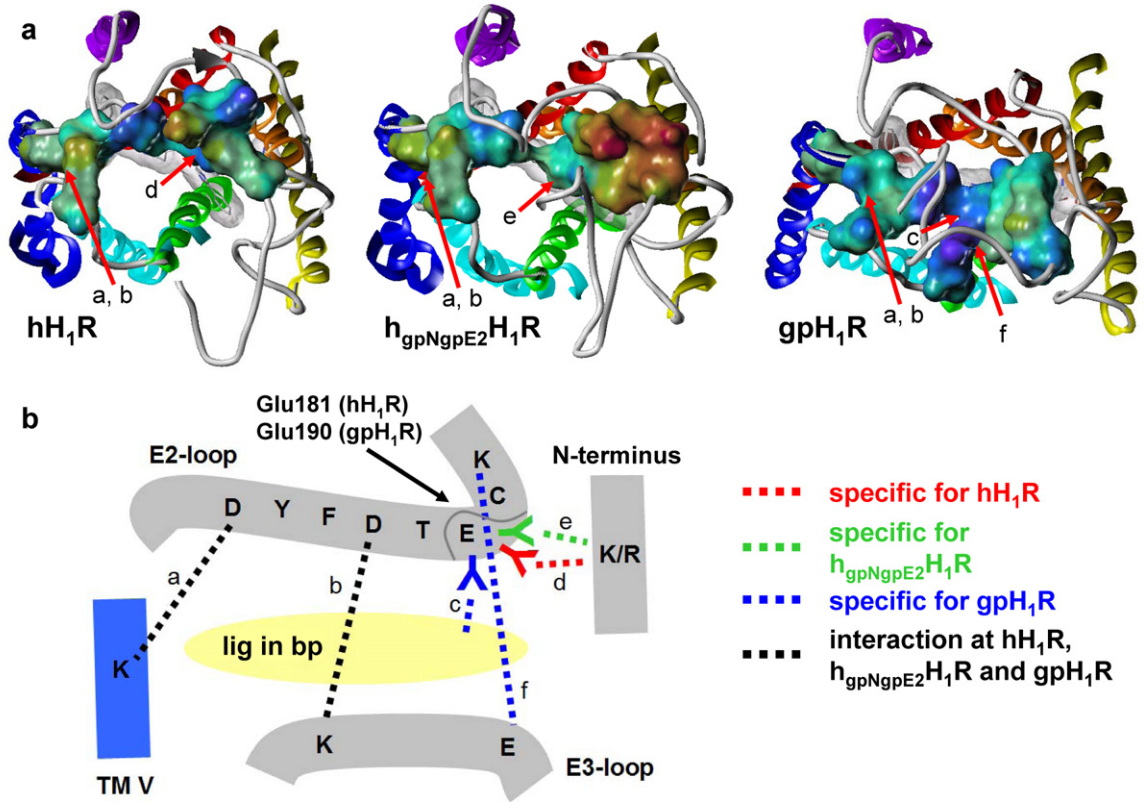

Fig. 7. Extracellular surface of hH_1R, $h_{gpNE2}H_1R$ and gpH_1R with phenoprodifen in the binding pocket. (a) Parts of the extracelluar surface, colored due to electrostatic potential; (b) scheme of stable electrostatic interactions on the extracellular surface. Stable electrostatic interactions at the extracellular surface at H_1R (numbering according to hH_1R, unless otherwise indicated): a: $K^{5.39}$–D186; b: D183–K442; c: E190 (gpH_1R)–Lig (gpH_1R); d: E181–K13; e: E190 ($h_{gpNgpE2}H_1R$)–R22 ($h_{gpNgpE2}H_1R$); f: K188 (gpH_1R)–E447 (gpH_1R). (For interpretation of the references to color in this figure legend, the reader is referred to the web version of the article.)

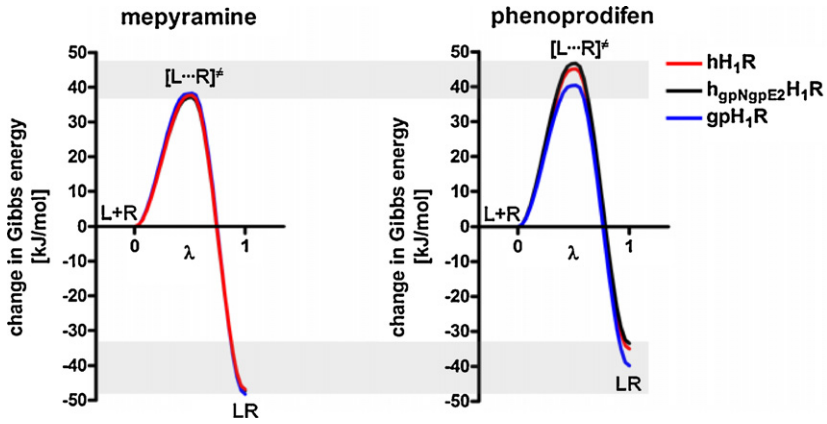

Fig. 8. Semi-quantitative diagrams presenting the change in Gibbs energy during ligand binding for mepyramine and phenoprodifen at hH_1R, $h_{gpNgpE2}H_1R$ and gpH_1R. The Gibbs energy diagrams are based on the data presented in Tables 2 and 4. For each system, the free ligand and free receptor (L + R) was used as reference and set to zero. Differences are indicated by the grey bars.

different entry points to the binding pocket for the ligand, and thus may influence rate constants of association. Additionally, there are different amino acids at hH_1R and gpH_1R at position 2.61, which directly points into the binding pocket (Fig. 6b) which could have an influence onto binding kinetics, too. Besides that, it has to be considered, that phenoprodifen is a partial agonist at H_1R. Consequently, it can be suggested, that conformational changes in the receptor may also have an influence onto binding kinetics.

4.3. Binding kinetics at H_1R

In Fig. 8, a semi-quantitative energy diagram with regard to changes in Gibbs energies during binding of mepyramine **1** and phenoprodifen **2** to hH_1R, $h_{gpNgpE2}H_1R$ and gpH_1R is shown. The diagram reveals that the Gibbs energy of activation for the binding of the antagonist mepyramine **1** is smaller than for the partial agonist phenoprodifen **2** at hH_1R, $h_{gpNgpE2}H_1R$ and gpH_1R. In contrast, the Gibbs energy of activation for ligand dissociation is higher for the antagonist mepyramine **1** than for the partial agonist phenoprodifen **2** at hH_1R, $h_{gpNgpE2}H_1R$ and gpH_1R. Two reasons may be responsible for these observations: Phenoprodifen **2** is a much more bulky ligand than mepyramine **1**. Thus, **2** may need more energy to find its way into the binding pocket. Additionally, in contrast to the partial agonist phenoprodifen **2**, mepyramine **1** is an antagonist. Thus, during binding of phenoprodifen **2**, the receptor has to change its conformation from the inactive to the active state. Thus, due to receptor activation, the $\Delta G^{\neq}_{ass}$ is higher for **2** than for **1**. Based on these data it may be suggested that $\Delta G^{\neq}_{ass}$ increases in the series antagonist → (partial) agonist. This is supported by the $\Delta G^{\neq}_{ass}$ values of the full agonist histamine **3** at hH_1R and gpH_1R. At hH_1R and gpH_1R, $\Delta G^{\neq}_{ass}$ is higher for the full agonist histamine **3**, than for the partial agonist phenoprodifen **2**. Based on the rate constants for mepyramine and levocetirizine, determined by Gillard et al. [23] at 25 °C, we calculated the corresponding Gibbs energies of activation: For mepyramine, $\Delta G^{\neq}_{ass}$ is about 35 kJ/mol, for desloratadine, $\Delta G^{\neq}_{ass}$ is about 43 kJ/mol, whereas for levocetirizine a $\Delta G^{\neq}_{ass}$ is about 47 kJ/mol. The $\Delta G^{\neq}_{ass}$ was found about 88 kJ/mol in case of mepyramine, and about 99 kJ/mol in case of desloratadine and levocetirizine. Thus, the Gibbs energies of activation, calculated based on the data of Gillard et al. [23] are in the same magnitude, as determined within this study, despite the differences in temperature. Mepyramine, desloratadine and levocetirizine are H_1R antagonists, thus, the Gibbs energy of activation is ligand-dependent.

Our results with regard to H_1R are in good accordance to the concept of differences in energy landscape, on the one hand in dependence of agonists or antagonists, on the other hand in dependence of ligand structure [33,34]. In recent studies, it was shown, that the extracellular loops are important with regard to ligand recognition and receptor activation, as summarized by Peeters et al. [35]. Furthermore, in sophisticated NMR studies it was experimentally shown for the $h\beta_2R$ that the extracellular surface is regulated in dependence of the bound ligand [25]. Using pharmacological, chimeric receptor and molecular modelling approaches for H_1R and H_4R we have shown that the extracellular surface has, in dependence of the ligand, influence onto affinity, potency and efficacy [7,24]. Additionally the extracellular part of H_1R has influence onto association kinetics of ligands. In our study, we identified a glutamate in the E2-loop (Glu181 at hH_1R, Glu190 at gpH_1R) to be involved in the interaction network on the extracellular surface of H_1R (Fig. 7). At $h\beta_2R$, Asp192 (E2-loop), at a corresponding position to Glu181 at hH_1R, was identified to be involved in salt bridge rearrangement during receptor activation [25]. This position is directly neighboured to the highly conserved cysteine, which establishes a disulfide bridge to TM III. Thus, due to the restrained position we assume that the amino acid in this position is a key residue on the extracellular surface of GPCRs.

5. Conclusion

Within this study we have analyzed the binding kinetics of mepyramine and phenoprodifen to hH_1R, gpH_1R and the chimera $h_{gpNgpE2}H_1R$. The data revealed species differences between hH_1R and gpH_1R in rate constants for association and dissociation. The experimental studies suggest that the association kinetics of the antagonist mepyramine and the partial agonist phenoprodifen are significantly different between hH_1R and the chimera $h_{gpNgpE2}H_1R$. Thus, we are, best to our knowledge, the first to show by competition binding kinetics, that the extracellular surface of the H_1R has an influence onto association kinetics of a ligand. This result may also be relevant for other biogenic amine receptors.

Acknowledgements

We thank G. Wilberg for cell culture. This work was supported by DFG (STR 1125/1-1) of the Deutsche Forschungsgemeinschaft.

References

[1] Moguilevsky N, Varsalona F, Noyer M, Fillard M, Fuillaume JP, Garcia I, et al. Stable expression of human H_1-histamine receptor cDNA in chinese hamster ovary cells. Pharmacological characterization of the protein, tissue distribution of messenger RNA and chromosomal localisation of the gene. Eur J Biochem 1994;224:489–95.

[2] Foord SM, Bonner TI, Neubig RR, Rosser EM, Pin JP, Davenport AP, et al. International union of pharmacology. XLVI. G protein-coupled receptor list. Pharmacol Rev 2005;57:279–88.
[3] Hill SJ, Ganellin CR, Timmerman H, Schwartz JC, Shankley NP, Young JM, et al. International union of pharmacology. XIII. Classification of histamine receptors. Pharmacol Rev 1997;49:253–78.
[4] Seifert R, Wenzel-Seifert K, Bürckstümmer T, Pertz HH, Schunack W, Dove S, et al. Multiple differences in agonist and antagonist pharmacology between human and guinea pig histamine H_1-receptor. J Pharmacol Exp Ther 2003;305:1104–15.
[5] Bruysters M, Jongejan A, Gillard M, van de Manakker F, Bakker RA, Chatelain P, et al. Pharmacological differences between human and guinea pig histamine H_1 receptors: Asn^{84} (2.61) as a key residue within an additional binding pocket in the H_1 receptor. Mol Pharmacol 2005;67:1045–52.
[6] Strasser A, Striegl B, Wittmann HJ, Seifert R. Pharmacological profile of histaprodifens at four recombinant histamine H_1 receptor species isoforms. J Pharmacol Exp Ther 2008;324:60–71.
[7] Strasser A, Wittmann HJ, Seifert R. Ligand-specific contribution of the N-terminus and E2-loop to pharmacological properties of the histamine H_1-receptor. J Pharmacol Exp Ther 2008;326:783–91.
[8] Strasser A, Wittmann HJ, Kunze M, Elz S, Seifert R. Molecular basis for the selective interaction of synthetic agonists with the human histamine H_1-receptor compared with the guinea-pig H_1-receptor. Mol Pharmacol 2009;75:454–65.
[9] Elz S, Kramer K, Pertz HH, Detert H, ter Laak AM, Kühne R, et al. Histaprodifens: synthesis, pharmacological in vitro evaluation, and molecular modelling of a new class of highly active and selective histamine H_1-receptor agonists. J Med Chem 2000;43:1071–84.
[10] Menghin S, Pertz HH, Kramer K, Seifert R, Schunack W, Elz S. N^{α}-Imidazolylalkyl and pyridylalkyl derivatives of histaprodifen: synthesis and in vitro evaluation of highly potent histamine H_1-receptor agonists. J Med Chem 2003;46:5458–70.
[11] Bruysters M, Pertz HH, Teunissen A, Bakker RA, Gillard M, Chatelain P, et al. Mutational analysis of the histamine H_1-receptor binding pocket of histaprodifens. Eur J Pharmacol 2004;487:55–63.
[12] Jongejan A, Leurs R. Delineation of receptor-ligand interactions at the human histamine H_1 receptor by a combined approach of site-directed mutagenesis and computational techniques-or-how to bind the H_1 receptor. Arch Pharm Chem Life Sci 2005;338:248–59.
[13] Strasser A. Wittmann HJ.3D-QSAR CoMFA study to predict orientation of suprahistaprodifens and phenoprodifens in the binding-pocket of four histamine H_1-receptor species. Mol Inf 2010;29:3333–41.
[14] Shimamura T, Shiroishi M, Weyand S, Tsujimoto H, Winter G, Katritch V, et al. Structure of the human histamine H_1 receptor complex with doxepin. Nature 2011;475:65–70.
[15] Rasmussen SGF, Choi HJ, Rosenbaum DM, Kobilka TS, Thian FS, Edwards PC, et al. Crystal structure of the human β_2 adrenergic G-protein-coupled receptor. Nature 2007;450:383–7.
[16] Rasmussen SGF, DeVree BT, Zou Y, Kruse AC, Chung KY, Kobilka TS, et al. Crystal structure of the β_2 adrenergic receptor–Gs protein complex. Nature, in press, doi:10.1038/nature10361.
[17] Wittmann HJ, Seifert R, Strasser A. Contribution of binding enthalpy and entropy to affinity of antagonist and agonist binding at human and guinea-pig histamine H_1-receptor. Mol Pharmacol 2009;76:25–37.
[18] Tran VT, Chang RSL, Snyder SH. Histamine H_1 receptors identified in mammalian brain membranes with [^{3}H]mepyramine. Neurobiology 1978;75:6290–4.
[19] Wallace RM, Young JM. Temperature dependence of the binding of [^{3}H]mepyramine and related compounds to the histamine H_1-receptor. Mol Pharmacol 1982;23:60–6.
[20] Treherne JM, Young JM. Temperature-dependence of the kinetics of the binding of [^{3}H]-(+)-N-methyl-4-methyldiphenhydramine to the histamine H_1-receptor: comparison with the kinetics of [^{3}H]-mepyramine. Br J Pharmacol 1988;94:811–22.
[21] Onaran HO, Bökesoy TA. Kinetics of antagonism at histamine-H_1 receptors in isolated rabbit arteries. Naunyn-Schmiedeberg's Arch Pharmacol 1990;341:316–23.
[22] Gillard M, van der Perren C, Moguilevsky N, Massingham R, Chatelain P. Binding characteristics of cetirizine and levocetirizine to human H_1 histamine receptor: contribution of Lys^{191} and Thr^{194}. Mol Pharmacol 2002;61:391–9.
[23] Gillard M, Chatelain P. Changes in pH differently affect the binding properties of histamine H_1 receptor antagonists. Eur J Pharmacol 2006;530:205–14.
[24] Brunskole I, Strasser A, Seifert R, Buschauer A. Role of the second and third extracellular loops of the histamine H_4 receptor in receptor activation. Naunyn-Schmiedeberg's Arch Pharmacol, in press, doi:10.1007/s00210-011-0673-3.
[25] Bokoch MP, Zou Y, Rasmussen SGF, Liu CW, Nygaard R, Rosenbaum DM, et al. Ligand-specific regulation of the extracellular surface of a G-protein-coupled receptor. Nature 2010;463:108–14.
[26] Houston C, Wenzel-Seifert K, Bürckstümmer T, Seifert R. The human histamine H2-receptor couples more efficiently to Sf9 insect cell Gs-proteins than to insect cell Gq-proteins: limitations of Sf9 cells for the analysis of receptor/Gq-protein coupling. J Neurochem 2002;80:678–96.
[27] Motulsky HJ, Mahan LC. The kinetics of competitive radioligand binding predicted by the law of mass action. Mol Pharmacol 1983;25:1–9.
[28] Eyring H. The activated complex in chemical reactions. J Chem Phys 1935;3:107–15.
[29] Laidler KJ, King MC. The development of transition state theory. J Phys Chem 1983;87:2657–64.
[30] Scheerer P, Park JH, Hildebrand PW, Kim YJ, Krauß N, Choe HW, et al. Crystal structure of opsin in its G-protein-interacting conformation. Nature 2008;455:497–503.
[31] Wittmann HJ, Seifert R, Strasser A. Nα-methylated phenylhistamines exhibit affinity to the hH4R—a pharmacological and molecular modelling study. Nauny-Schmiedeberg's Arch Pharmacol, in press, doi:10.1007/s00210-011-0671-5.
[32] Ballesteros JA, Shi L, Javitch JA. Structural mimicry in G protein-coupled receptors: implications of the high-resolution structure of rhodopsin for structure-function analysis of rhodopsin-like receptors. Mol Pharmacol 2011;60:1–19.
[33] Kobilka BK, Deupi X. Conformational complexity of G-protein-coupled receptors. Trends Pharmacol Sci 2007;28:397–406.
[34] Deupi X, Kobilka BK. Energy landscapes as a tool to integrate GPCR structure, dynamics and function. Physiology (Bethesda) 2010;25:293–303.
[35] Peeters MC, van Westen GJP, Li Q, Ijzerman AP. Importance of the extracellular loops in G protein-coupled receptors for ligand recognition and receptor activation. Trends Pharmacol Sci 2011;32:35–42.